Evaluation of Uncertainties due to Hydrogeological Modeling and Groundwater Flow Analysis - Effective Continuum Model Using TOUGH2

Christine Doughty and Kenzi Karasaki

Earth Sciences Division
E.O. Lawrence Berkeley National Laboratory

Abstract

Starting with regional geographic, geologic, hydrologic, geophysical, and meteorological data, we develop an effective continuum model to simulate subsurface flow and transport in a 4 km by 6 km by 3 km thick fractured granite rock mass overlain by sedimentary layers. Individual fractures are not modeled explicitly. Rather, continuum permeability and porosity distributions are assigned stochastically, based on well-test data and fracture density measurements. Large-scale features such as lithologic layering and major fault zones are assigned deterministically. We employ the TOUGH2 simulator for the flow calculation. The model simulates the steady-state groundwater flow through the site, then streamline analysis is used to calculate travel times for particles leaving specified monitoring points to reach the boundary of the model. Model results for the head distribution compare favorably with head profiles measured in several deep boreholes and the overall groundwater flow is consistent with regional water balance data. Predicted travel times range from 1 to 25 years.

1. INTRODUCTION

The Japan Nuclear Cycle Development Institute (JNC) has initiated a multi-national project to investigate the uncertainties involved in the prediction of flow and transport behavior of a fractured rock mass. In the initial stage of the project, the H-12 flow comparison, several research organizations conducted numerical simulations with the same starting information regarding tracer transport through a hypothetical fractured rock mass (Oyamada and Ikeda, 1999). The groups' results were compared to identify and quantify the uncertainties in the model predictions. The present stage of the project takes a similar approach, but considers a real field site, a 4 by 6 by 3 km region surrounding the MIU site in the Tono area of Gifu, Japan. The main results of the different groups' models are the predicted travel times from specified monitoring points to the model boundary. There are no comparable field data available to directly validate the models, so, as in the first stage, model uncertainty is assessed by comparing among results of different models.

We believe that this is potentially a very fruitful exercise. We do not believe, however, that there is much to gain in comparing how computer codes solve algebraic equations. A larger and often overlooked uncertainty lies in the development of the conceptual model. Another source of uncertainty that is tightly related to the development of the conceptual model lies in site characterization. The choice of field tests to be performed and how tests are designed, executed, and interpreted can have a strong effect on the resulting conceptual model, and ultimately on predictions made with the model.. For example, in the H-12 flow comparison, data were provided in a form tailored for a discrete fracture network model, making development of an effective continuum model cumbersome. In contrast, in the present stage data are presented in a more basic form, enabling a variety of conceptual models to be developed on equal footing. A major potential benefit of the present project is the chance for differences in model predictions to highlight aspects of site characterization that need to be improved in order to increase confidence in the model predictions, thus guiding the direction of ongoing site characterization activities.

In our conceptual model, a stochastic permeability distribution is used to represent fractured rock as an effective continuum. Individual fractures are not modeled explicitly. However, large-scale

features such as fault zones, lithologic layering, natural boundaries, and surface topography are incorporated deterministically. We think the geometric data of individual fractures are useful, but we only regard them as "soft data." The reasons are as follows: (1) It is virtually impossible to test individual fractures to measure and determine their transmissivity in the field. Therefore, the fracture transmissivity quoted in the literature is invariably inferred from borehole flow tests by making certain assumptions regarding the flow geometry. The measured value is likely to be the effective transmissivity of a collection of interconnected fractures at unknown distances and directions. (2) Fractures are in general neither planer, circular, nor square. (3) Variability of the hydraulic conductance (transmissivity) within a fracture is likely to be larger than the variability among fractures. (4) Correlation between the parameterized fracture geometry (e.g., fracture density and orientation) and the hydraulic properties of fractured rock mass may or may not exist.

Furthermore, even if accurate information on the flow and transport properties of individual fractures were available, there is only a limited spatial regime in which modeling individual fractures (a discrete fracture network model) is useful. At small scales or low fracture densities, the few individual fractures present may be modeled explicitly, but it is quite likely that there will be no connected fracture flow path across the model. At large scales and high fracture densities, the many fractures present are likely to be quite well connected, and thus more efficiently represented as an effective continuum. For the present problem the model extent (4 by 6 by 3 km) is far greater than the typical measured fracture spacing (8 per meter). Thus, we chose to construct an effective continuum model to simulate the groundwater flow and tracer transport.

In the sections below, we first introduce the numerical simulators used for the calculations. We then describe the available data and the steps used to build the numerical model. Next, we illustrate typical model results and tabulate selected results for multiple realizations. We conclude with suggestions for additional site characterization and model development.

2. METHODOLOGY

TOUGH2 simulator

The numerical simulator TOUGH2 (Pruess, 1987, 1991) is used for the flow calculations. TOUGH2 is a general-purpose code that simulates two-phase flow of air and water in gaseous and liquid phases together with tracer and heat transport through porous or fractured geologic media, which may be strongly heterogeneous. Depending on the design of the grid, TOUGH2 can represent individual fractures or fracture networks explicitly or through an effective continuum formulation, as is done here. The only limitation is that Darcy's law governs fluid flow through both the fractures and rock matrix, with relative permeability and capillary pressure functions used to describe the interactions between liquid and gas phases.

For the present work, we employ a simplified equation of state module known as EOS9 (Wu et al., 1996) that considers only a single component (water) under isothermal conditions (20^{o}C). When pressure conditions remain above 1 atm, single-phase liquid conditions prevail and the variable used to describe the state of the system is liquid pressure. If pressure declines below 1 atm, unsaturated conditions develop and the state variable becomes liquid saturation. Water viscosity is essentially constant under isothermal conditions, whereas in reality viscosity would be about four times smaller at the bottom of a 3 km thick rock block than at the top (assuming temperatures near 20^{o}C near the surface and a typical geothermal temperature gradient of 3^{o}C/100 m). If deep rocks have significant permeability, viscosity variability could have important ramifications for large-scale flow patterns.

TOUGH2 uses the integral-finite-difference method (IFDM) for spatial discretization (Edwards, 1972; Narasimhan and Witherspoon, 1976), which offers greatly increased flexibility in grid design

compared to typical finite difference methods. Grid blocks can be of arbitrary shape and size, and can be connected to as many neighboring grid blocks as desired. There need be no reference to a global system of coordinates, or to the dimensionality of a particular flow problem. For a regular lattice of grid blocks the IFDM is equivalent to a block-centered finite difference scheme, making it possible to simulate one-, two-, or three-dimensional rectangular geometries, or problems with radial, cylindrical, or spherical symmetry, in addition to more complicated irregularly arranged grid blocks. For the present work, we use a regular rectangular grid with non-uniform vertical spacing. Each grid block has a porosity and permeability value assigned to it, as described below.

Tecplot streamtraces

The commercial graphics package Tecplot is used to determine groundwater travel times from the flow field calculated by TOUGH2. These travel times consider transport due to advection only; no diffusion or dispersion is included. Tecplot displays streamtraces originating from 24 specified monitoring points (four depths at each of six locations). A utility program takes the information recorded by Tecplot along each streamtrace (location, flow rate, velocity, permeability, and porosity) and calculates streamtrace length, travel time to the model boundary, exit point on the boundary, and the mean and standard deviation of permeability and porosity along the streamtrace.

Available data and grid generation

We start with a regular 3D TOUGH2 grid of total extent 4.4 by 5.9 by 3.75 km (x (E-W) from 3600 m to 8000 m; y (N-S) from –71300 m to –65400 m; z (masl) from –3000 m to 375 m). The basic grid block size is a 100 m by 100 m by 100 m cube. This size was chosen to be comparable to the typical length of the open interval during well tests. Grid block thickness decreases to 50 m between z = 0 masl and the top of the model at z = 375 masl, to enable better representation of surface topography changes. Grid block thickness gradually increases below z = -1000 masl since no data are available to constrain the model (the deepest well extends only to z = -750 masl) and flow variability is expected to be gradual at depth. The dimensions of the grid are 44 by 59 by 23, for a total of 59,708 grid blocks.

Next, we trim the grid laterally to reproduce the irregular 4by 6 km model boundary that follows natural topographic boundaries such as ridgelines and the Toki River. This process removes 15,985 grid blocks. Then, we trim the grid vertically to match surface topography, as given by a 20 m by 20 m resolution digital topography map (dtm). This process removes an additional 4,323 grid blocks, leaving a total of 39,400 in the final grid.

We include the following features of interest deterministically by assigning grid blocks to different material types, depending on their (x,y,z) coordinates:

- The Tsukiyoshi fault is represented as a plane with location and orientation inferred from the surface trace, borehole occurrences, and seismic profiles. Several smaller surface lineaments identified from satellite or aerial images that are also identified in boreholes are modeled explicitly as well.
- Lithofacies changes observed in boreholes are kriged to form surfaces. These surfaces provide the boundaries between different material types in the model.
- The sediment/bedrock boundary inferred from EM studies is used as the boundary between the uppermost granite (Biotite) and the lowermost sedimentary rock (Toki-lignite bearing rock).

The resulting model is shown in Figure 1.

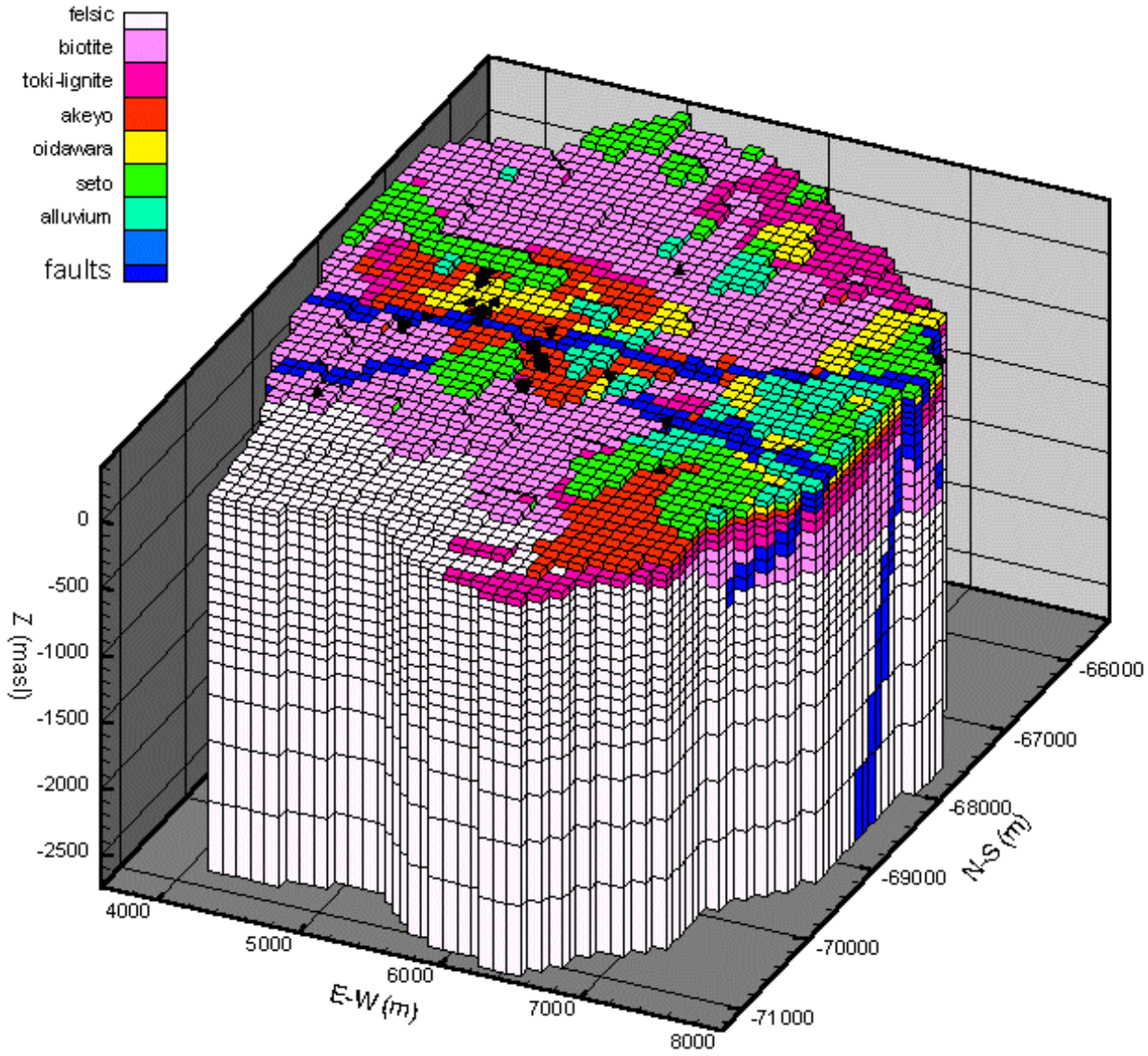

Figure 1. 3-D perspective view of the model used for the TOUGH2 simulations. Surface locations of wells are shown as black symbols.

Property assignment

Each grid block represents an effective fractured continuum with permeability and porosity assigned stochastically based on field measurements. Permeability is proportional to hydraulic conductivity K. K is determined from slug tests and pumping tests conducted using packed-off intervals in boreholes. Because many of the intervals used for the tests are of the same order as the grid block size, we assume that there is no need to scale up or scale down K values measured during well tests, and that they directly represent effective continuum conductivities. Grid block conductivity values are drawn from random distributions for each material type. The distributions are constructed by resampling field measurements, unless there are not enough measurements for a given material type to make resampling viable, in which case a log-normal distribution is used. Table 1 summarizes the material types and conductivity distributions used for the model and Figure 2 illustrates the $\log_{10}$K distributions that are constructed by resampling. For the granitic rocks and fault zones, weighting conductivity values by the length of the test interval shifts the distributions toward higher conductivities, implying that long test intervals are likely to be associated with high conductivity values. If test intervals are chosen to reflect features observed in the rock, then this relationship supports the concept that high-conductivity fractures tend to be more spatially extensive than low-conductivity fractures.

Table 1. Summary of material properties used in the model. The mean values of $\log_{10}$K shown in parentheses correspond to the distributions shown in the left-hand column of Figure 2 and are not used.

Material Type	Number of conductivity measurements	$\log_{10}$K (m/s)		Type of distribution used for $\log_{10}$K	
		Mean	S.D.		
Alluvium	0	–7.9*	1.6*	Normal	
Seto group	0	–7.9*	1.6*	Normal	
Oidawara	1	–8.7	1.6*	Normal	
Akeyo	11	–7.9 (–7.8)	0.8	Resampled	
Toki lignite-bearing	21	–7.0 (–6.7)	0.9	Resampled	
Biotite granite	192	–7.1 (–8.1)	1.7	Resampled	
Felsic granite	46	–6.9 (–7.4)	1.1	Resampled	
Faults	12	–7.7 (–7.9)	1.0	Tsukiyoshi resampled; other faults normal	
Material Type	Number of fracture density measurements	Fracture density (m^{-1})		Model Porosity	
		Mean	S.D.	Mean	S.D.
Biotite granite	57	7.7	4.2	3.9E-4	5.9E-4
Felsic granite	4	10.8	4.2	3.5E-4	2.7E-4
Overall	67	7.9	5.0	3.2E-4	4.2E-4
*No data available, use mean value for entire model					

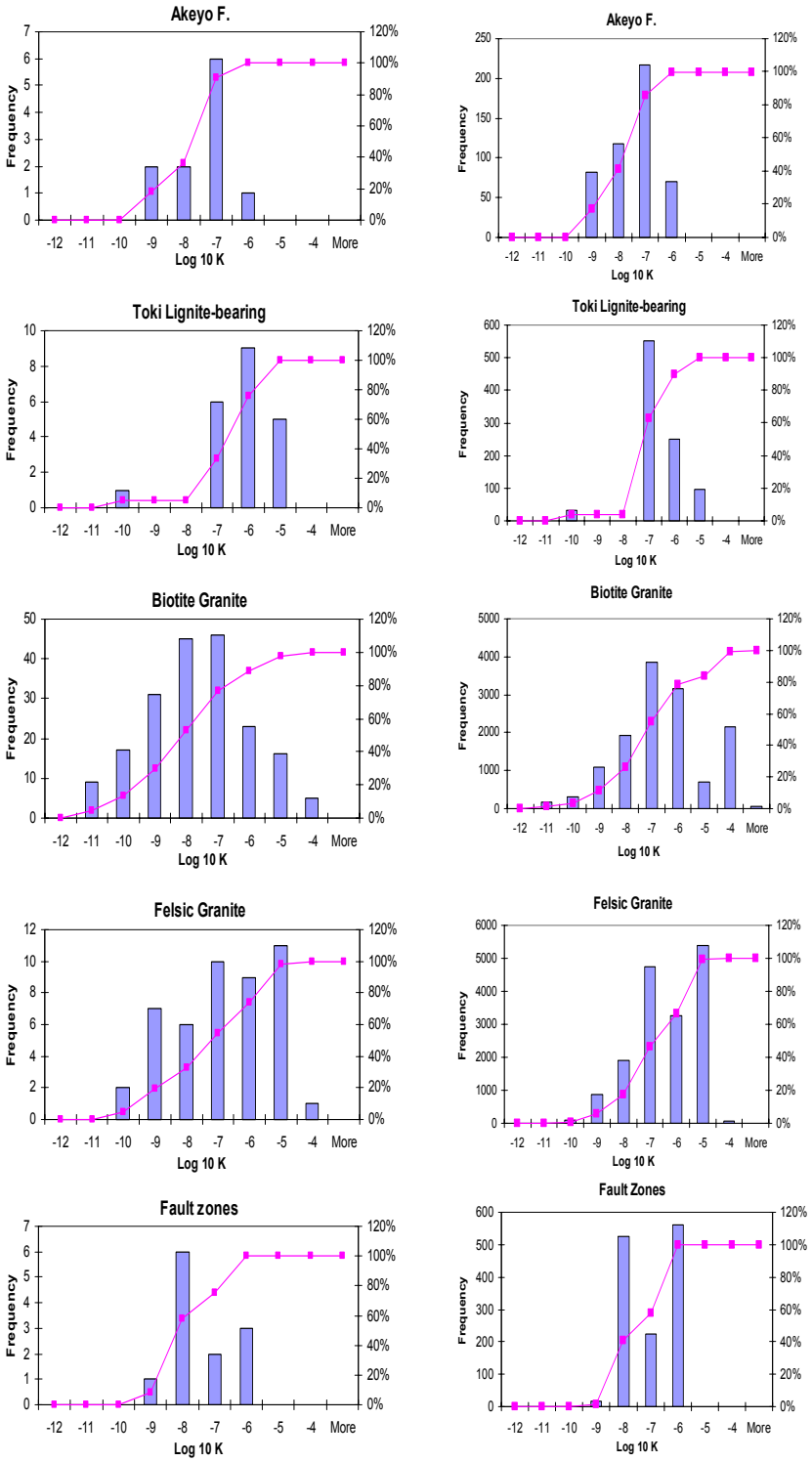

Figure 2. The left-hand column shows distributions of $\log_{10}K$ obtained from slug tests and pumping tests, with each test result equally weighted (i.e., counted once), regardless of the length of test interval used. In the right-hand column, each conductivity value is weighted by the length of test interval; frequency shows the number of grid blocks that are assigned a conductivity in the corresponding range.

Porosity ϕ is calculated as the product of fracture aperture w and fracture density d, with aperture determined from K and d using the cubic law:

$$\phi = w\, d = (12\, K\, \mu / d)^{1/3}\, d = (12\, K\, \mu\, d^2)^{1/3}. \quad (1)$$

Note that effective continuum conductivity K is related to the actual conductivity of an individual fracture K_f according to $K = K_f\, w\, d$.

Fracture density measurements are sparse and there is no obvious correlation between fracture density and conductivity, so fracture density measurements from all lithological layers are combined to determine a mean fracture density of 7.95 m^{-1} and a standard deviation of 5 m^{-1}. For most of the lithological layers, fracture densities are drawn from a normal distribution with these moments, which is truncated at a small positive number (0.01 m^{-1}) to ensure that fracture density is always positive. However, for the Biotite and Felsic granites, fracture density distributions are created by resampling density measurements from that lithofacies.

For each grid block, after K and d have been drawn from the appropriate distribution, Equation (1) is applied to determine ϕ. The resulting model porosity statistics are summarized in Table 1. Note that ϕ must be positive, but that the standard deviation is typically the same magnitude as the mean, implying that the ϕ distribution arising from Equation (1) is distinctly non-normal.

Model porosity is considered to be less well constrained than model conductivity for several reasons. First, basing porosity estimates on fracture density measurements is problematic because a high percentage of observed fractures may not contribute to flow at all. Moreover, the cubic law can greatly misrepresent the relationship between fracture aperture and conductivity, and even if it is valid, the hydraulic aperture used in the cubic law tends to underestimate the volumetric aperture relevant for transport. Finally, there are very few fracture density measurements available for materials other than the Biotite granite. Note that no data whatsoever are available for depths below 1000 m. Hence, all model properties there are quite uncertain.

Boundary conditions

- Surface topography guides us in determining the nature of the lateral boundary conditions for shallow portions of the model: the model is closed along ridgelines, whereas constant-head boundaries exist in a valley to the northeast and along the Toki River at the model's southern edge (Figure 3). However, it is unknown how deep these boundary conditions should be applied. It may be that at great depths, local surface topography has little or no effect on regional groundwater flow, and larger-scale, regional topographic trends determine appropriate boundary conditions. In the absence of any actual data, we assign the constant-head boundaries shown in Figure 3 over most of the depth of the model.
- The bottom of the model is closed. In the three deepest layers of the model, below the depths of any field data, the permeability of the model gradually decreases. This is intended to reproduce a gradual closing of fractures due to the increase in lithostatic pressure with depth.
- The top of the model is held at a head value equal to the surface elevation, to represent a near-surface water table. Flow from the constant head boundary into the model represents subsurface recharge. This configuration eliminates the need to model percolation through the vadose zone, which is a highly non-linear process and hence computationally intensive.
- The Tono mine is represented as a mass sink at the sedimentary/bedrock interface, with a constant strength equivalent to 1500 m^3/month, determined by time-averaging outflow measurements at the mine.

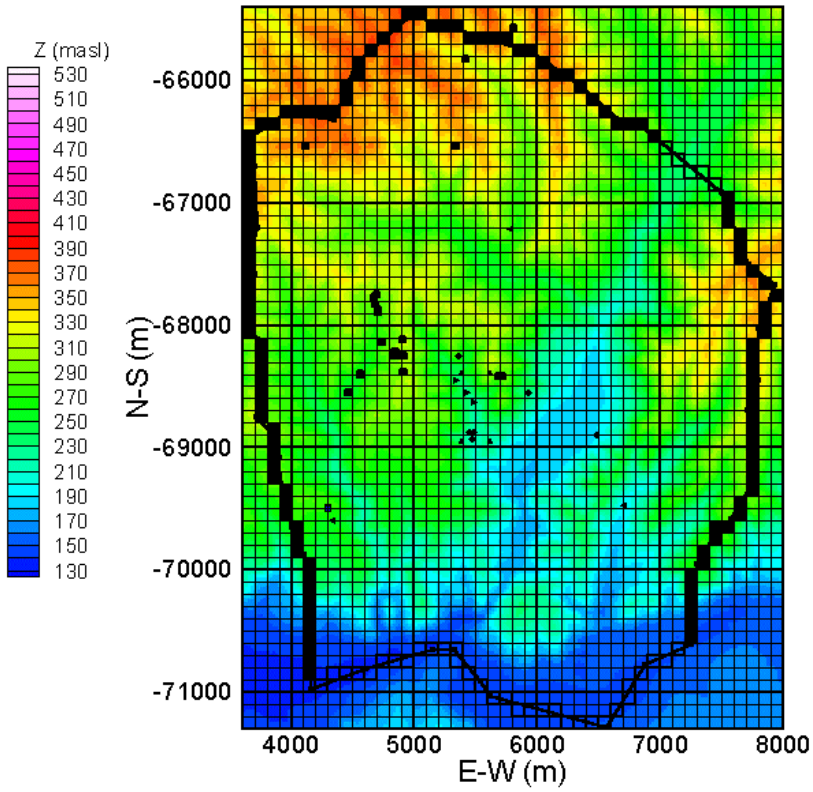

Figure 3. Plan view of the model's lateral boundary, superimposed on the digital topography map of the area. Closed boundaries are shown as filled-in black squares and constant-head boundaries are shown as open squares. Smaller black symbols identify well locations.

3. RESULTS

We model steady-state flow with TOUGH2, then trace streamlines from monitoring points with Tecplot. Results of preliminary sensitivity studies that were used to choose the boundary conditions are described first, followed by results for our chosen base case, an alternative case with lower permeability in the Tsukiyoshi fault, and a subsequent sensitivity study on the boundaries representing rivers.

Preliminary boundary condition variations

In these sensitivity studies, permeability and porosity are uniform within each material type rather than being drawn from random distributions, to more clearly illustrate the effects of alternative boundary conditions.

Thickness of lateral constant-head boundaries

How deep to apply the constant-head boundaries is a major point of uncertainty. Figure 4a illustrates the effect of limiting the constant-head portion of the lateral boundaries to the 250 m just below the ground surface. The shape of the flow paths away from the monitoring points and the location at which they leave the model is much different than in Figure 4b, where nearly the entire height of the model is open. Careful thought is required in order to choose appropriate boundary conditions for a large model such as the present one, in which surface effects may or may not be significant at great depths.

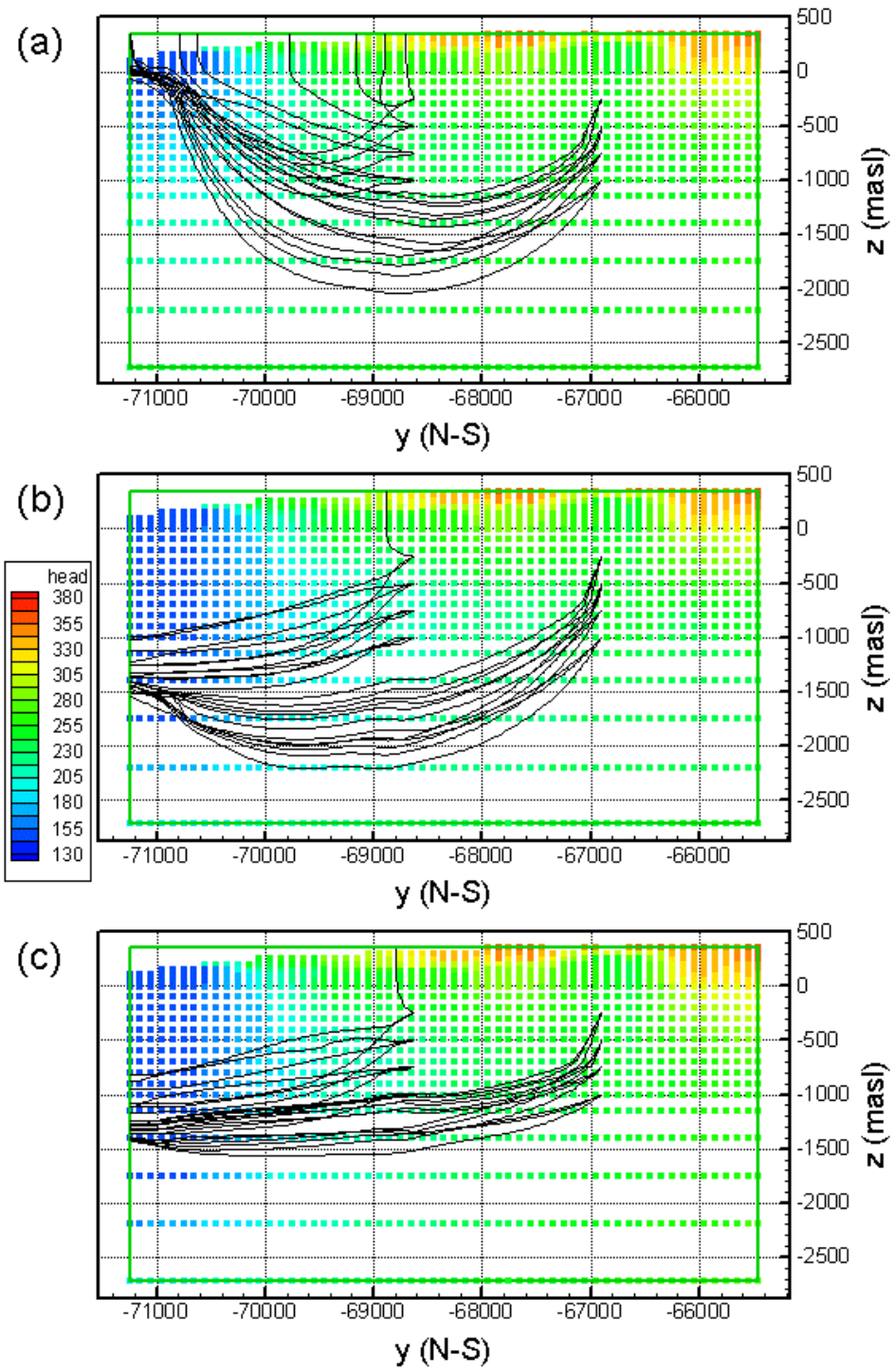

Figure 4. North-south cross-sectional (y-z) view of the streamtraces from the monitoring points. All x (E-W) values are projected on a single plane. In (a) the lateral constant-head boundaries extend less than 500 m below the ground surface; in (b) and (c) they extend over all but the lowest two layers of the model. In (c) the permeability in each of the lowest three layers is three times smaller than the permeability above it.

Nature of closed lower boundary

It is often expected that permeability should decrease as depth increases, due to increasing lithostatic pressure that tends to close fractures, pore spaces, or other fluid flow paths. No such trend was observed in the well test data collected, but the model extends more than 2 km below the deepest well penetration. Figures 4a and 4b show models with no permeability decrease with depth, but in Figure 4c, permeability in each of the bottom three layers decreases by a factor of three from the permeability above it. This gradual permeability decrease serves to limit fluid flow in the deepest portion of the model, making the lower no-flow boundary a gradational boundary rather than an abrupt one. If permeability does in fact decrease with depth, the choice of lateral flow boundary conditions at depth becomes less critical, as little fluid flow occurs there regardless of the boundary conditions applied.

Multiple realizations of base case

Our base case includes the features shown in Figure 4c: lateral constant-head boundary conditions that extend over most of the model thickness and a gradual decrease in permeability at depth, because we believe these are reasonable choices. However, there is no direct evidence to support them, and as illustrated in Figure 4, they have important ramifications for fluid flow paths.

The base case simulation was conducted for uniform permeability and porosity within each material type and for 10 realizations of random permeability and porosity distributions. Figure 5 shows the permeability distribution and streamtraces originating at the 24 monitoring points for one of the realizations. Simplified water balances for each realization are presented in Table 2. The recharge quantity is about a factor of two smaller than the value inferred from rainfall, evaporation, and streamflow data. Most of the outflow is to or below the Toki River, but a small fraction leaves the model through a small low-elevation section to the northeast. Based on the topography of the surrounding area, this may not be reasonable, and is further investigated below. There is a marked difference between uniform and random permeability distributions, with significantly more water moving through the system for random permeability fields. We expect that if spatially correlated random fields were used, throughflow would be even larger.

Table 2. Simplified water balances for the base case realizations. Quantities are all in kg/s with surface recharge converted to mm/yr shown in parentheses.

Case	Surface recharge	Outflow at Tono mine	Outflow through northeast boundary segment	Outflow through Toki River boundary segment
J74 (non random)	39.5 (68)	0.57	3.4	35.5
J74R	57.2 (98)	0.57	4.4	52.2
J74S	60.7 (104)	0.57	3.5	56.7
J74T	56.1 (96)	0.57	3.8	51.7
J74U	61.1 (104)	0.57	7.2	53.4
J74V	59.9 (102)	0.57	4.0	55.3
J74W	61.3 (105)	0.57	9.8	50.9
J74X	62.4 (107)	0.57	8.7	53.2
J74Y	55.4 (95)	0.57	5.2	49.6
J74Z	59.3 (101)	0.57	4.0	54.8
J74A	58.5 (100)	0.57	2.7	55.2

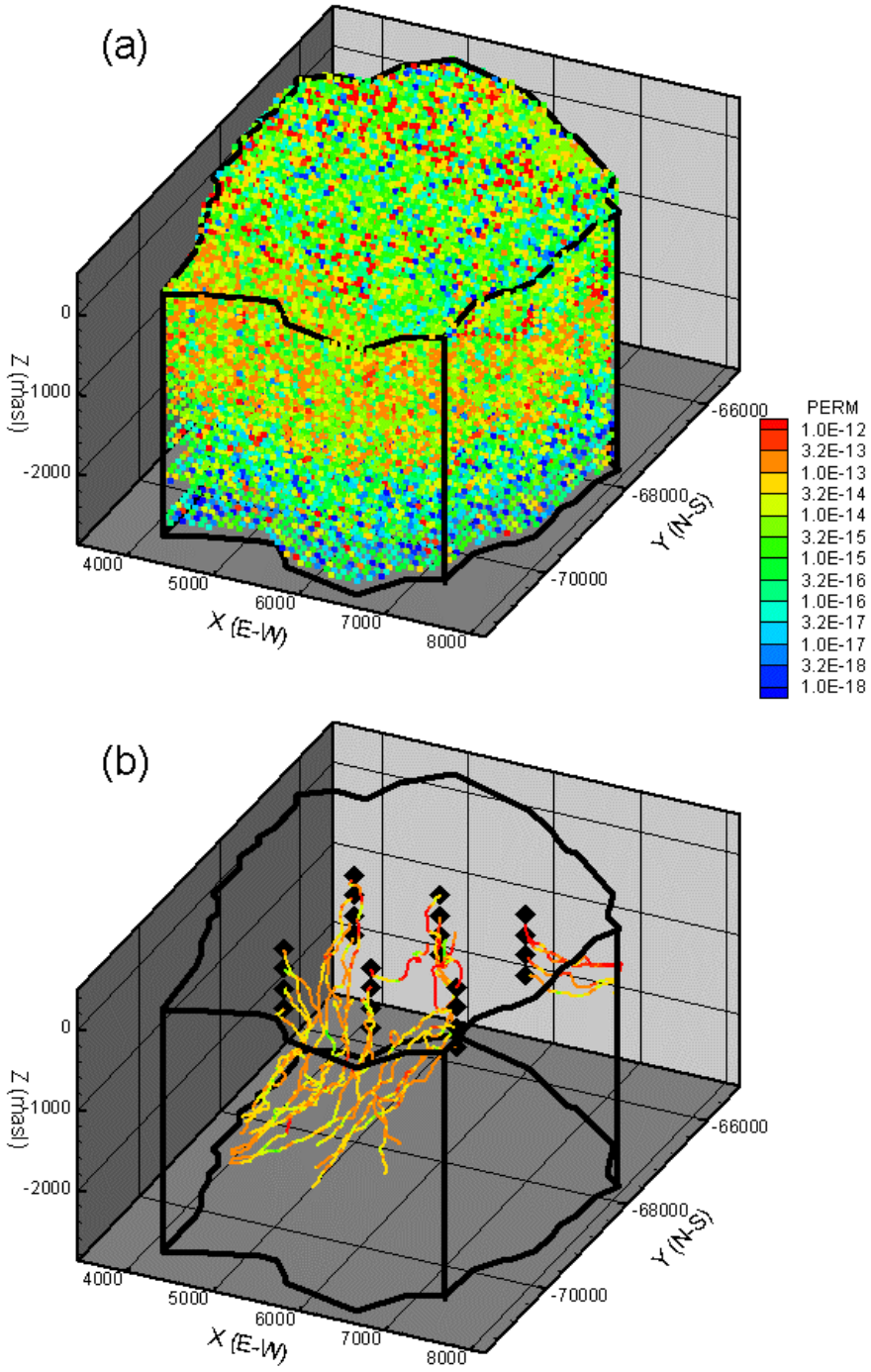

Figure 5. Permeability distribution (a) for the whole model and (b) along the streamtraces, for realization J74R of the base case. Monitoring points at which streamtraces originate are shown as black diamonds. Permeability in m^2 is approximately 10^{-7} times conductivity in m/s.

Table 3 shows an example of the information collected along streamtraces for each realization, including starting and ending location, path length, travel time, and a statistical description of the conductivity and porosity along the path. The streamtraces are highly irregular and the average permeability along the flow paths is greater than that of the model as a whole, illustrating preferential flow along high permeability pathways. The large standard deviations for $\log_{10}K$ and ϕ reflect the high variability along the flow paths. Travel time from the monitoring points to the model boundary ranges from 1 to 16 years, with an average travel time of 7 years. The average velocity along the streamtraces is about 400 m/yr.

Table 3. Streamtrace information for base case realization J74R.

Starting location			Number of points on stream-trace	$\log_{10}K$ (m/s)		Porosity		Path length (m)	Travel time (yrs)	Ending location			Avg velocity (m/yr)
x_0 (m)	y_0 (m)	z_0 (m)		Mean	Stdev	Mean	Stdev			x_f (m)	y_f (m)	z_f (m)	
4489	-66900	-250	160	-6.04	0.58	3.7E-04	2.1E-04	5029	15.6	5380	-70760	-988	322
4489	-66900	-500	146	-6.14	0.45	3.7E-04	1.5E-04	4635	10.7	5188	-70679	-1298	435
4489	-66900	-750	144	-6.06	0.46	3.9E-04	1.5E-04	4552	11.1	5217	-70656	-1470	411
4489	-66900	-1000	131	-6.29	0.54	3.5E-04	1.5E-04	4247	14.8	5185	-70670	-1306	286
5489	-66900	-250	79	-5.51	0.83	3.8E-04	2.8E-04	2487	6.3	6418	-68502	349	397
5489	-66900	-500	158	-6.00	0.35	4.1E-04	1.6E-04	5068	12.2	6801	-71066	-694	416
5489	-66900	-750	153	-6.10	0.48	4.0E-04	1.6E-04	4951	10.4	6076	-71158	-1240	477
5489	-66900	-1000	150	-6.27	0.48	3.6E-04	1.5E-04	4807	14.4	6036	-71165	-1478	334
6489	-66900	-250	42	-5.4	0.61	3.7E-04	2.7E-04	1306	6.5	7293	-66747	-761	201
6489	-66900	-500	33	-5.22	0.45	4.9E-04	2.3E-04	1028	2.1	7318	-66745	-783	494
6489	-66900	-750	33	-5.70	0.43	4.5E-04	1.5E-04	1073	1.5	7251	-66743	-988	736
6489	-66900	-1000	30	-6.16	0.45	4.3E-04	1.9E-04	931	1.6	7236	-66743	-1059	568
4489	-68629	-250	79	-6.23	0.33	3.0E-04	1.0E-04	2565	4.6	5231	-70660	-805	559
4489	-68629	-500	84	-6.11	0.44	4.3E-04	1.7E-04	2708	3.4	5196	-70671	-1249	786
4489	-68629	-750	80	-6.24	0.37	3.8E-04	1.5E-04	2444	3.3	5158	-70674	-867	736
4489	-68629	-1000	80	-6.12	0.31	3.9E-04	1.7E-04	2571	3.3	5140	-70672	-1027	787
5489	-68629	-250	113	-5.29	0.99	3.3E-04	2.4E-04	1905	8.2	6250	-68849	348	232
5489	-68629	-500	95	-6.16	0.51	4.1E-04	2.0E-04	3034	6.6	6077	-71169	-793	461
5489	-68629	-750	83	-6.07	0.33	4.3E-04	1.8E-04	2531	4.7	5540	-70955	-942	535
5489	-68629	-1000	88	-6.22	0.46	3.6E-04	1.3E-04	2750	6.3	5408	-70862	-1392	438
6489	-68629	-250	26	-5.67	1.12	4.1E-04	2.7E-04	743	0.9	6388	-68690	347	865
6489	-68629	-500	42	-5.53	1.07	5.7E-04	4.9E-04	1183	2.1	6410	-68782	349	567
6489	-68629	-750	88	-6.12	0.39	3.9E-04	1.6E-04	2777	6.5	6085	-71170	-952	429
6489	-68629	-1000	89	-6.10	0.40	4.2E-04	1.6E-04	2831	8.5	6784	-71054	-1106	331
Average over all streamtraces				-5.95		4.00E-04		2840	6.9				412
Minimum over all streamtraces				-6.29		3.00E-04		743	0.9				201
Maximum over all streamtraces				-5.22		5.70E-04		5068	15.6				865

Table 4 compares streamtrace information among all the different base case realizations. The variation between the different random realizations is relatively small, which is not surprising considering that the quantities being compared already represent average behavior over the different streamtraces of each realization.

Table 4. Average streamtrace information for all base case

Base Case Realizations	$Log_{10}K$	Porosity	Length (m)	Travel time (yr)	Velocity (m/yr)
J74 (non-ramdom)	-6.93	3.5E-04	3292	11.4	289
J74R	-5.95	4.0E-04	2840	6.9	412
J74S	-5.92	4.4E-04	3148	7.2	435
J74T	-5.93	4.2E-04	3090	8	386
J74U	-5.88	4.3E-04	3150	8.5	371
J74V	-6.05	3.9E-04	3246	8	404
J74W	-5.98	4.0E-04	2703	5.8	467
J74X	-5.94	4.3E-04	3255	8.3	394
J74Y	-5.93	4.4E-04	2928	7.5	392
J74Z	-5.97	4.1E-04	2863	6.2	459
J74A	-5.88	4.5E-04	2948	8.1	364
Average over 10 random realizations	-5.94	4.2E-04	3017	7.5	408
Std dev.	0.05	1.9E-05	178	0.9	33

Multiple realizations of low-permeability Tsukiyoshi fault case

Although conductivity values determined for fault zones do not appear to be significantly different than those for granitic rocks (see Table 1), observed head increases below the Tsukiyoshi fault suggest that it may act as a low-permeability barrier to flow. To test this hypothesis, we consider a case in which the permeability of grid blocks representing the Tsukiyoshi fault is decreased by a factor of ten. Water balances are shown in Table 5; they do not differ significantly from the base case.

Table 5. Simplified water balances for the low-permeability Tsukiyoshi fault case. Quantities are all in kg/s with surface recharge converted to mm/yr shown in parentheses.

Case	Surface recharge	Outflow at Tono mine	Outflow through northeast boundary segment	Outflow through Toki River boundary segment
J75 (non random)	38.0 (65)	0.57	5.1	32.3
J75R	56.6 (97)	0.57	6.2	49.8
J75S	59.1 (101)	0.57	4.8	53.7
J75T	54.7 (94)	0.57	4.9	49.3

Figure 6 shows head profiles at the location of Well MIU-2 for some of the realizations of the above two cases. Although there is a great deal of variability between the different realizations, the effect of assigning lower permeability to the Tsukiyoshi fault results in an obvious increase in head below the fault depth. Figure 7 shows an example of the streamtraces leaving the monitoring points. The general flow pattern is similar for the two cases, but the effect of decreasing permeability in the Tsukiyoshi fault is apparent in the less direct paths illustrated by the streamtraces for that case.

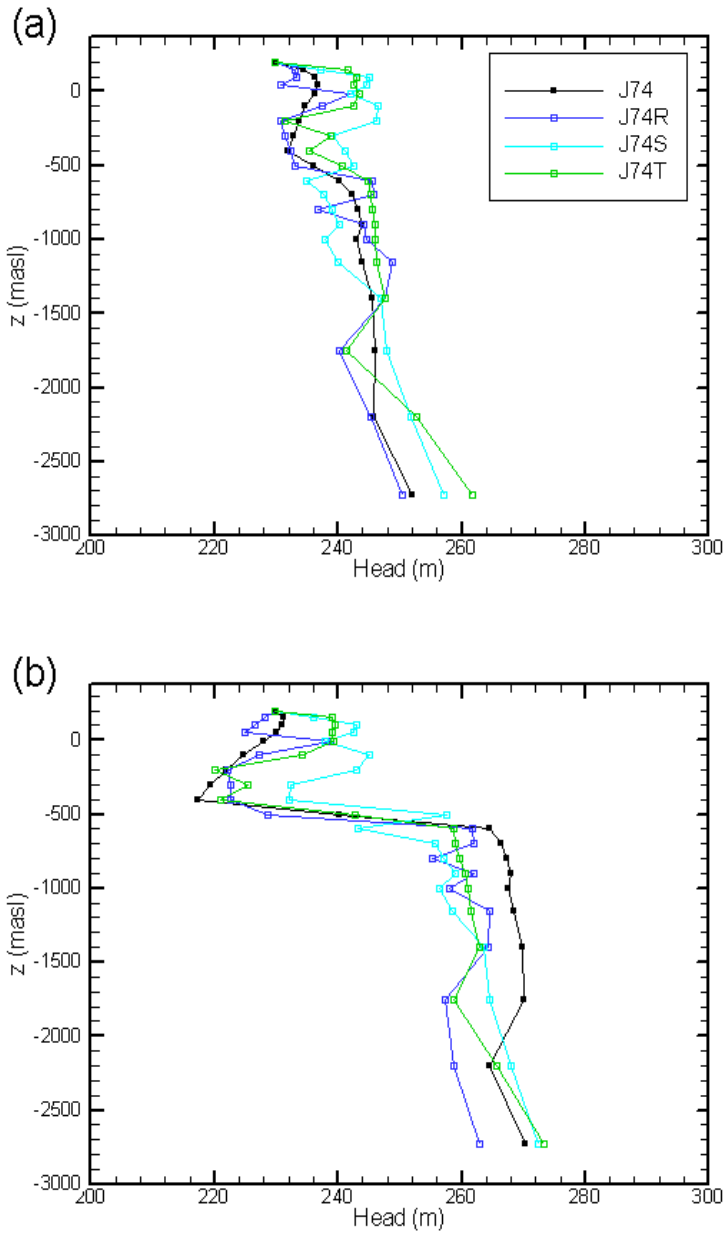

Figure 6. Head profiles at the location of Well MIU-2 for (a) the base case; and (b) the low-permeability Tsukiyoshi fault case. Cases J74R, J74S, and J74T represent different realizations of a random property distribution; Case J74 has uniform properties within each material type.

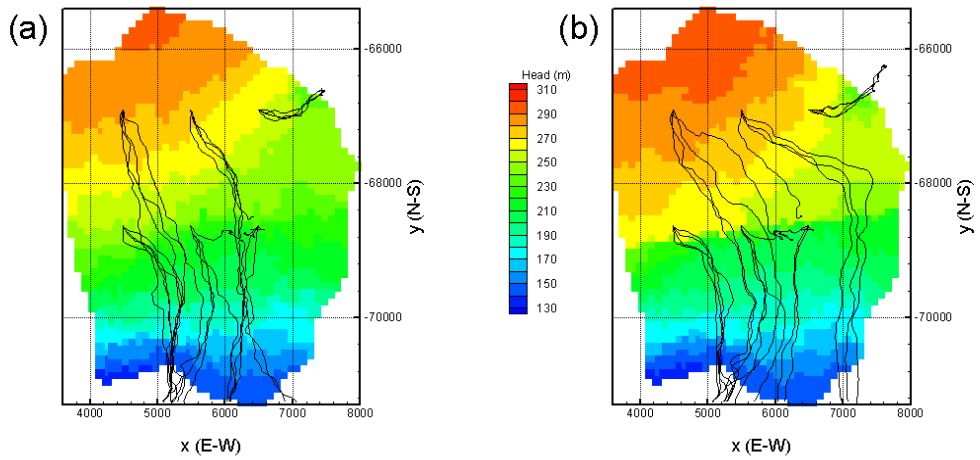

Figure 7. Streamtraces and head distributions for (a) the base case and (b) the low-permeability Tsukiyoshi fault case. The 3D streamtraces are projected to the model top surface. The head distribution is for z = -1000 masl.

Table 6 compares streamtrace information among all the different realizations of the low-permeability Tsukiyoshi fault case. As for the base case, the variation between the different random realizations is relatively small. Moreover, the differences between the base case and the low-permeability Tsukiyoshi fault case are also minor, with average travel time increasing slightly, from 7 to 9 years.

Table 6. Average streamtrace information for all low-permeability Tsukiyoshi fault realizations.

Low-K Tsukiyoshi Fault Realizations	$Log_{10}K$	Porosity	Length (m)	Travel time (yr)	Velocity (m/yr)
J75 (non-random)	-6.96	3.5E-04	2751	12.1	228
J75R	-5.91	4.0E-04	2914	10.2	287
J75S	-5.94	4.2E-04	3074	8.5	362
J75T	-5.86	4.4E-04	2998	8.8	342
Average over 3 random realizations	-5.90	4.2E-04	2995	9.2	330
Standard deviation	0.04	2.0E-05	80	0.9	39

Variation of head levels at boundaries representing rivers

We varied the head level of the northeast constant-head boundary to study its effect on both the local flow paths in that region and the overall water balance. Table 7 summarizes the water balances for the cases considered and Figure 8 shows some of the streamtraces. Based on the larger-scale topography, we believe that the cases in which there is inflow to the model rather than outflow from the model through the northeast boundary are more reasonable. Assuming a 10 m head increase at the boundary is equivalent to assuming that the water table at the boundary is quite near the ground surface, whereas throughout the rest of the model the water table depth averages 10 m. Borehole measurements throughout the area suggest that an average water-table depth of 10 m is reasonable and the presence of a river intersecting the open northeast boundary makes a shallower water table there plausible. It is possible that assigning a similar increase in head at the Toki River boundary along the southern edge of the model may also be appropriate. As shown in Table 7, this change has a strong effect on the overall water balance. Further investigation of the local topography around the northeast model boundary and the Toki River model boundary is needed to determine how best to assign river boundary conditions.

Table 7. Simplified water balances for different river boundary conditions. Quantities are all in kg/s with surface recharge converted to mm/yr shown in parentheses.

Case	Surface recharge	Outflow at Tono mine	Outflow through NE boundary segment*	Outflow through Toki River boundary segment
Base case (J74R)	57.2 (98)	0.57	4.4	52.2
Add 5 m to head at northeast boundary	55.0 (94)	0.57	2.2	52.3
Add 10 m to head at northeast boundary	52.8 (90)	0.57	-0.2	52.4
Add 15 m to head at northeast boundary	50.3 (86)	0.57	-2.8	52.5
Add 10 m to head at northeast and Toki River boundaries	30.0 (51)	0.57	-0.02	29.6

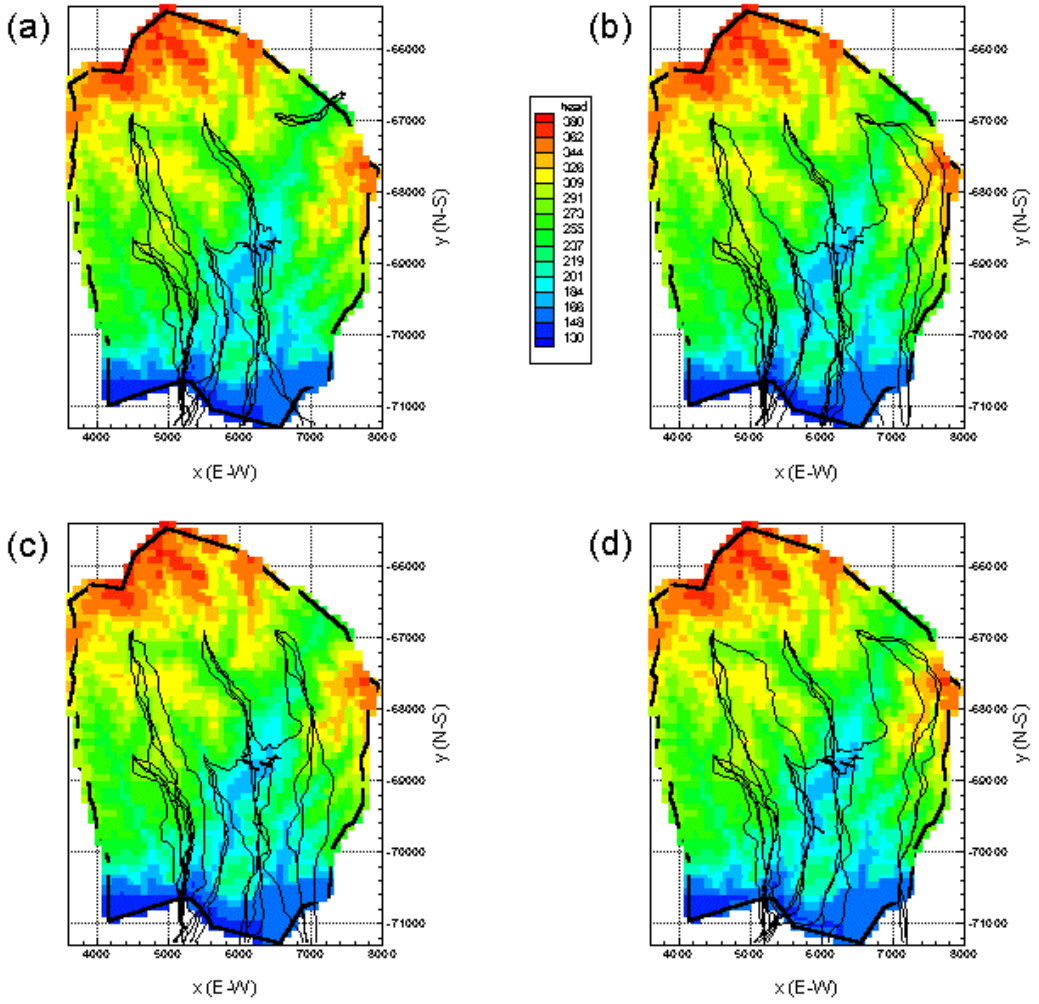

Figure 8. Plan view of streamtraces for a realization of the base case (J74R) with different head boundary conditions at the open boundaries: (a) the original head boundary condition; (b) a head increase of 10 m at the northeast boundary; and (c) a head increase of 15 m at the northeast boundary; and (d) a head increase of 10 m at the northeast boundary and at the Toki River boundary

4. CONCLUSIONS

We have used a variety of surface and subsurface data to build a hydrologic flow and transport model of the 4 by 6 km region surrounding the MIU site. No one type of data provides enough information by itself, but each contributes to the overall effort. Table 8 summarizes how different data have been used so far, and proposes some potential future uses.

After a preliminary sensitivity study on model boundary conditions, a base case was chosen and 10 realizations of the stochastic permeability and porosity distributions were created. Three realizations of a variation considering a lower permeability in the Tsukiyoshi fault were also created.

Model results suggest that the average travel time from the monitoring points to the model boundary is relatively short for both cases: about 7 years for the base case and about 9 years for the low-permeability Tsukiyoshi fault case. Decreasing the permeability in the Tsukiyoshi fault causes noticeable changes in the pressure profile near the fault, but not a wholesale change in flow pattern through the model.

For each case, there is significant variability among the different stochastic realizations in terms of the details of the streamtrace patterns, including model exit locations. However, if only average results such as the mean travel time or mean path length are considered, then variability among realizations is relatively small. Greater variability arises from imposing different boundary conditions or assigning low permeabilities to the Tsukiyoshi fault and deep model layers, emphasizing the need to establish a sound basis for determining these model properties. Another highly uncertain model parameter is the effective porosity, to which travel time estimates are very sensitive. The following subsections describe areas where further work would help reduce uncertainty in model predictions.

Additional data needed

To better characterize the regional water balance, in particular the role of the shallow sedimentary layers in connecting surface infiltration and the underlying granitic basement, the following data would be useful:

- The hydrologic character of the sedimentary layers (i.e., is flow fracture-dominated?); conductivity and porosity values for shallow layers. Recharge estimates over a wider area (quantitative or qualitative information)
- The Toki River gain or loss over the model boundary
- Data on the river at the NE constant-head model boundary
- Other big contributors to the regional water balance (e.g., golf course irrigation)

Possible additional site characterization

To better quantify the permeability and porosity distributions used in the model, the following site characterizations activities would be valuable:

- Isotope or other naturally occurring tracers (to estimate residence or travel times between various regions, to get a better understanding of regional groundwater flow)
- Active tracer tests (to help constrain the estimation of fracture porosity)
- Longer-term pumping tests (most of conductivity information comes from slug tests, which may be less reliable than pumping tests)

- Cross-hole well tests (to develop a better understanding of fracture connectivity)

Table 8. Summary of data used to develop the 4x6 km model.

Data Type	Actual Use	Potential Use
Landsat images	Qualitative understanding of regional surface topography	Improve lateral model boundaries at great depths
Surface topography	Provide detailed topography that impacts shallow groundwater flow	
Seismic profiles	Locate faults in 2-D sections	
Electrical resistance	Provide spatially extensive image of the sediment/bedrock boundary	
Surface geological map	Verify granite outcrop locations in model	Improve assignment of shallow material types, especially among sedimentary rocks
Water balance data	Estimate average surface recharge into the model	Identify locations of especially large or small recharge
Wellbore lithologies	Assign material types	
Wellbore fracture identification	Determine stochastic distribution of fracture density for use in calculation of model porosity	
Well tests	Provide distributions of conductivity values for model	Use in inversion to determine conductivity of specific regions
Multi-packer monitoring	Investigate connectivity and flow barriers	Same as well tests
Drillers' notes		Identify high flow zones
Flow and temperature logs		Investigate regional groundwater flow

Additional model development needed

In the present model development, the surface geology was not used to constrain assignment of model properties. This could readily be done, but it would require a finer vertical resolution to be used near the surface for the model to accurately represent surface geology. For such a grid refinement to be a useful exercise, more information on the sedimentary rock properties is needed.

At depth, the lateral boundaries may not be strongly related to the surface topography, as they are near the surface. A means of assigning different lateral boundary conditions at different depths is needed. Additionally, the outflow from the NE boundary of the model seems inconsistent with the larger scale surface topography. Although the quantity of flow is small, it is worthwhile to investigate what changes are needed to replace this outflow with an inflow.

Correlated random fields may be helpful to properly represent preferential flow, as high- or low-permeability regions greater than 100 m in extent (the grid block size) are likely to exist.

Bands of increased permeability surrounding the Tsukiyoshi fault have been suggested, based on tectonic concepts. The model could be modified to incorporate such bands, and proposed long-term pumping tests could be modeled to estimate their permeability

Information obtained during drilling (e.g., depths of lost fluid) and temperature and flow meter logs may be useful for identifying major flow paths, which can be added to the model deterministically. This information may also improve our understanding of the regional groundwater flow.

Running a non-isothermal version of the model to evaluate the effect of geothermal temperature increases on water density and viscosity would be useful. It might even be possible to provide

constraints on deep permeabilities by comparing modeled and observed borehole termperature profiles.

ACKNOWLEDGMENTS

This work was supported by Japan Nuclear Fuel Cycle Corporation (JNC) and Taisei Corporation of Japan. through the U.S. Department of Energy Contract No. DE-AC03-76SF00098. We are particularly indebted to Mr. Atsushi Sawada of JNC and Mr. Yuji Ijiri.of Taisei Corp. for useful discussions. We would also like to thank Mr. Shinji Takeuci and Mr. Hiromitsu Saegusa for making various field data available to us. The authors would like to thank Dr. Stefan Finsterle for his critical review.

REFERENCES

Edwards, A.L., TRUMP: A computer program for transient and steady state temperature distributions in multidimensional systems, National Technical Information Service, National Bureau of Standards, Springfield, VA, 1972.

Narasimhan, T.N. and P.A. Witherspoon, An integrated finite difference method for analyzing fluid flow in porous media, Water Resources Res., 12(1), 57-64, 1976.

Oyamada, K. and T. Ikeda, Uncertainty analysis on hydrologic modeling in heterogeneous media (CORE Collaborative Study), Japan Nuclear Fuel Cycle Development Institute TJ1400 99-023, 1999.

Pruess, K., TOUGH user's guide, Rep. LBL-20700, Lawrence Berkeley Laboratory, Berkeley, CA, 1987.

Pruess, K., TOUGH2 – A general-purpose numerical simulator for multiphase fluid and heat flow, Rep. LBL-29400, Lawrence Berkeley Laboratory, Berkeley, CA, 1991.

Wu, Y.S., C.F. Ahlers, P. Fraser, A. Simmons and K. Pruess, Software qualification of selected TOUGH2 modules, Rep. LBNL-39490, Lawrence Berkeley National Laboratory, Berkeley, CA, 1996.